sMILE: The First MIMO Envelope Detection Testbed

Georgios K. Psaltopoulos, Christoph Sulser, and Armin Wittneben
Communication Technology Laboratory, ETH Zurich, CH-8092 Zurich, Switzerland
Email: {psaltopoulos, csulser, wittneben}@nari.ee.ethz.ch

***Abstract*—We present the first implementation of a MIMO envelope detection system. Such systems have so far been theoretically studied in the framework of nonlinear MIMO. The design considered employs an envelope detector on each receive antenna. The simplicity of the receiver enables extreme low-cost low-power implementations, making such systems attractive for wireless sensor networks and alike applications. The testbed presented here is a first implementation of such a system and demonstrates detection of spatially-multiplexed data streams using envelope detectors.**

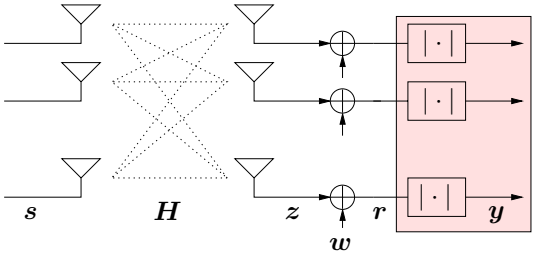

Fig. 1. MIMO Envelope Detection System Model.

I. Introduction

We consider multiple-input multiple-output (MIMO) systems where the receiver has *access only to the amplitude* (envelope) of the complex-valued received signal. This implies that the receiver does not require the ubiquitous I/Q structure, but a simple *envelope detector* suffices instead. Power-intensive circuitry like a mixer and precise local oscillator reference are not necessary, and hence implementation of such a receiver is extremely low-power [1]. This type of design is especially suited for wireless sensor networks or alike systems, where low complexity and low power consumption have highest priority. The MIMO envelope detector has been studied in the framework of *nonlinear MIMO systems* in [2], [3], [4] and [5]. The nonlinearity refers to the operation of extracting the envelope of the complex-valued received signal.

The information-theoretic limits of nonlinear MIMO systems for the case of perfect or noisy channel state information (CSI) at the receiver have been investigated in [2]. The performance and diversity order of the maximum likelihood (ML) detector of MIMO systems with envelope detectors were studied in [3] for the case of perfect CSI. Several estimation schemes have been developed in [4] and [5]. The available work offers the basic knowledge required for building a MIMO envelope detector.

In this paper we present the first MIMO enveLope dEtection (sMILE) testbed. Our goal is to demonstrate detection of spatially multiplexed data streams using multiple envelope detectors, under realistic propagation conditions. For the purpose of the testbed we have designed and constructed several envelope detector receivers that operate concurrently and act as a single multiple antenna receiver. We show that a very simple receiver design comprising very basic components suffices for a MIMO envelope detector system. Optimizing the power consumption of the receiver is out of the scope of this work, since this is achieved through integration into a system on chip. The testbed enables validation and benchmarking of the detection and channel estimation schemes that have been derived in previous works, as well as development of practical aspects that are required in an implementation, e.g. synchronization. Using the testbed we can test the validity of the assumptions made by the theoretical model in a practical implementation. This separates the implementation-imposed characteristics from the fundamental properties that drive MIMO envelope detectors, giving precious insights into the nature of MIMO envelope detection.

In Section II we briefly describe the theoretical system model and the work conducted so far. In Section III we describe the testbed components and operation, while in Section IV we comment on measurement results.

II. System Description

The theoretical system model is depicted in Fig. 1. The symbol $\boldsymbol{s} \in \mathcal{S}$ is transmitted from N_{T} transmit antennas and captured by N_{R} receive antennas. The channel $\boldsymbol{H}$ is assumed to be frequency flat block fading. The received vector $\boldsymbol{z} \in \mathbb{C}^{N_{\mathrm{R}}}$ is perturbed by a zero-mean circularly symmetric Gaussian noise vector $\boldsymbol{w} \in \mathbb{C}^{N_{\mathrm{R}}}$. Subsequently, an envelope detector *on each* receive antenna extracts the amplitude $\boldsymbol{y}$ of the complex valued received signal $\boldsymbol{r}$. The detector has access *only* to $\boldsymbol{y}$.

Modulation: Since the phase of the received signal is neglected by the envelope detectors, information can be conveyed only through the amplitude of the transmit signal. We assume that independent On-Off Keying (OOK) data streams are transmitted on every antenna, such that $\boldsymbol{s} = \{0, \sqrt{2E_s/N_{\mathrm{T}}}\}^{N_{\mathrm{T}}}$, where E_s is the average symbol energy. The uncoded bit rate is N_{T} bits/symbol.

ML Detection: The ML detector has been studied in [3]. The detector assumes perfect knowledge of the channel matrix

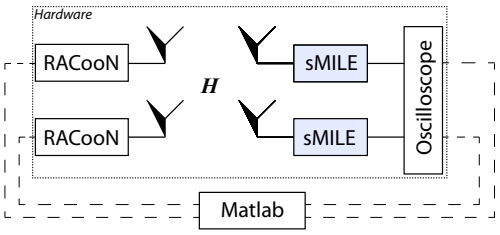

Fig. 2. sMILE testbed hardware block diagram (here for a 2×2 MIMO system). Dashed lines correspond to software 'connections'.

$\boldsymbol{H}$ and maximizes the conditional pdf of the received signal as follows:

$$\begin{aligned}\widehat{\boldsymbol{s}}_{\mathrm{ML}} &= \underset{\boldsymbol{s}\,\in\,\mathcal{S}}{\operatorname{argmax}}\, \mathrm{p}(\boldsymbol{y}|\boldsymbol{z}) = \underset{\boldsymbol{s}\,\in\,\mathcal{S}}{\operatorname{argmax}} \prod_{i=1}^{N_{\mathrm{R}}} \mathrm{p}\left(y_i|z_i\right) \\ &= \underset{\boldsymbol{s}\,\in\,\mathcal{S}}{\operatorname{argmax}} \prod_{i=1}^{N_{\mathrm{R}}} \frac{2y_i}{\sigma_w^2} e^{-\frac{y_i^2+|\boldsymbol{e}_i^{\mathrm{T}}\boldsymbol{H}\boldsymbol{s}|^2}{\sigma_w^2}} \mathrm{I}_0\left(\frac{2y_i\left|\boldsymbol{e}_i^{\mathrm{T}}\boldsymbol{H}\boldsymbol{s}\right|}{\sigma_w^2}\right) \quad (1)\end{aligned}$$

where $\boldsymbol{e}_i$ is the ith column of the identity matrix. Eq. (1) is the product of Rician distributions due to envelope detection. Note that the Rician distribution becomes a Rayleigh distribution when the hypothesis z_i equals zero.

Channel Estimation: Estimating the complete complex-valued channel matrix $\boldsymbol{H}$ is not possible using only envelope detectors. However, the *hypotheses* required by the ML detector in (1), i.e. the quantities $|\boldsymbol{e}_i\boldsymbol{H}\boldsymbol{s}|$, can in fact be estimated by a MIMO envelope detector, since they have the form of the *norm* of sums of channel coefficients. The set of all required hypotheses $\mathcal{X}$ is called the *sufficient CSI*, indicating that knowledge of $\mathcal{X}$ is sufficient for ML detection. E.g., for $N_{\mathrm{T}} = 2$, $E_s = 1$ and $\boldsymbol{s} \in \{0,1\}^2$, the hypotheses are: $|h_{11}|, |h_{12}|, |h_{21}|, |h_{22}|$, $|h_{11}+h_{12}|$ and $|h_{21}+h_{22}|$. The problem of estimating the sufficient CSI has been studied in [4] and [5], and three estimation schemes have been proposed: SEES, GAES and ARES. These three schemes have different performance characteristics and pilot-length scaling properties. For each scheme, a certain set of pilot symbols is repeated N_{scheme} times each. The total pilot length is then given by

$$N_{\mathrm{tot}}^{\mathrm{SEES}} = (2^{N_{\mathrm{T}}} - 1) \cdot N_{\mathrm{SEES}} \quad (2)$$

$$N_{\mathrm{tot}}^{\mathrm{GAES}} = \frac{1}{2} N_{\mathrm{T}}(N_{\mathrm{T}}+1) \cdot N_{\mathrm{GAES}} \quad (3)$$

$$N_{\mathrm{tot}}^{\mathrm{ARES}} = (3N_{\mathrm{T}} - 2) \cdot N_{\mathrm{ARES}} \quad (4)$$

and is a function of the number of transmit antennas N_{T}.

III. sMILE Testbed

The sMILE testbed is an implementation of the above theoretical system model and includes the aforementioned ML detector and channel estimation schemes. A general block diagram of the testbed setup is given in Fig. 2 for the case of 2×2 MIMO envelope detection. Two *custom programmable wireless nodes*, RACooN's, serve as transmitters[1]. The RACooN's are set to transmit independent OOK streams concurrently at $f_c = 5.6$ GHz, simulating this way a virtual multiple antenna transmitter. The receiver consists of independent sMILE nodes. These nodes are simple custom-made envelope detectors that yield the envelope of the received signal on every receive antenna. The received envelopes are recorded on a digital oscilloscope. Subsequently, the signals are read out and further processed in Matlab.

[1]The RACooN nodes are part of our lab equipment for simulating relaying protocols [6].

TABLE I
sMILE transmit signal parameters.

Description	Value
Symbol/bit sampling frequ./period	$f_s = 1$ MHz, $T_s = 1$ μs
Symbols per packet (example)	$N_{\mathrm{SpP}} = 250$
Packet duration	$T_{\mathrm{packet}} = N_{\mathrm{SpP}} T_s = 250$ μs
Packets per burst	$N_{\mathrm{packet}} = 102$ symbols
Burst duration	$T_{\mathrm{burst}} = N_{\mathrm{packet}} T_{\mathrm{packet}} = 25.5$ ms
Typical synchronization length	$N_{\mathrm{sync}} = 11$ symbols (Barker code)
Typical repetitions of pilot bits	$N_{\mathrm{pilot}} = 10$ symbols
Typical data length	$N_{\mathrm{data}} = N_{\mathrm{SpP}} - N_{\mathrm{sync}} - N_{\mathrm{pilot}} = 229$ sym
Total pilot length	$N_{\mathrm{tot}}^{\mathrm{pilot}}$ symbols, see (2), (3) and (4)
RACooN sampling frequ./period	$f_{\mathrm{RCN}} = 80$ MHz, $\mathrm{T}_{\mathrm{RCN}} = 12.5$ ns
Transmit pulse	Nyquist-pulse, $\beta = 1$, length $6T_s$
Transmit signal bandwidth	$W_{\mathrm{bb}} = 1$ MHz, $W_{\mathrm{pb}} = 2$ MHz

A. Transmit Signal

The RACooN's can transmit bursts of maximum duration 25.5 ms. Every burst is split into packets, each comprising a *synchronization sequence*, a *pilot sequence* and a *data payload*. First, a transmit burst is generated at symbol frequency $f_s = 1$ MHz and then convolved with a Nyquist-pulse at the RACooN sampling frequency $f_{\mathrm{RCN}} = 80$ MHz. The resulting 'continuous-time' burst is uploaded to the RACooN's. Table I summarizes the various parameters of the transmit signal.

The synchronization sequence can be chosen between a length 11 Barker code or a length 31 m-sequence. The pilot is constructed according to the chosen estimation scheme, SEES, GAES or ARES (cf. [5]).

B. sMILE Nodes

The sMILE nodes are simple envelope detection nodes. In essence, this operation can be performed without the need of down-conversion. The absence of the mixer and the LO would lead to tremendous power and cost savings in such a design. However, we are constrained to implement our receiver at 5.6 GHz. For practical reasons, we will first down-convert the received signal at an IF of $f_{\mathrm{IF}} = 305$ MHz, where a larger selection of more efficient components is available.

Fig. 3 depicts an abstract block model of the sMILE nodes. The receiver has a very straightforward structure. First, the received signal at the antenna is bandpass filtered at RF and then amplified by an LNA. The RF signal is subsequently mixed with a free-running LO carrier, obtained by a VCO. The resulting IF signal is first amplified and then sharply filtered by a surface acoustic wave (SAW) bandpass filter. Finally, the filtered IF signal is fed to a *Received Signal Strength Indicator* (RSSI) detector, which outputs the baseband signal V_{out}. The circuit could as well be implemented *only* with an amplifier, a bandpass and an RSSI detector, if the carrier frequency was lower. Table II summarizes the components employed.

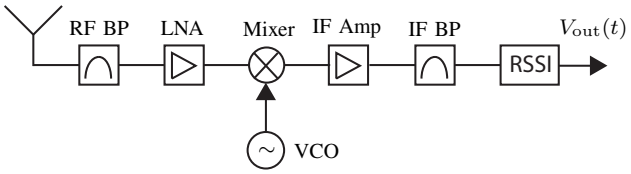

Fig. 3. Block diagram of sMILE nodes.

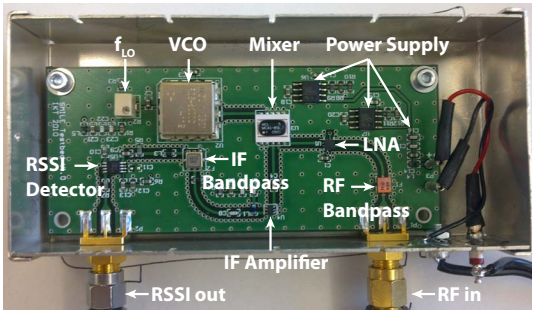

Fig. 4. Picture of sMILE node #0.

The heart of the sMILE node is the RSSI detector. This component is based on a logarithmic amplifier and outputs a baseband signal which follows the envelope of the received signal, albeit in a logarithmic scale. The RSSI detector corresponds to the envelope detection block of Fig. 1. Although RSSI detectors have usually an auxiliary role and drive the automatic gain control (AGC) circuitry, they are the actual data detectors in this design. This further stresses the low-cost/low-complexity potential of our receiver. Logarithmic RSSI detectors have a very high dynamic range. This is necessary in our application, since we use OOK. That is, we need to distinguish between a high level, dependent on the channel strength, and a low level which corresponds to no-signal/noise-only. Logarithmic amplifiers are not characterized by a single noise figure. We delve into the noise characteristics of the sMILE nodes in Section III-D.

A total of 5 sMILE nodes have been built for the purposes of our testbed. Each node consumes approximately 90 mA. Fig. 4 depicts a picture of the first node #0. The circuit is mounted in a metallic box that offers both mechanical stability and isolation from electromagnetic interference.

The measured I/O characteristics of the sMILE nodes are given in Fig. 5 and can be approximated as a linear function of the input power $P_{\text{in}}^{\text{RF}}$:

$$V_{\text{out}} = V_{\text{slope}} \cdot \left(P_{\text{in}}^{\text{RF}} - P_0\right) \quad [\text{mV}]. \tag{5}$$

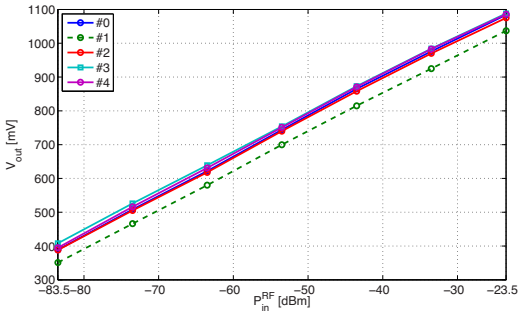

Fig. 5. I/O characteristic of all sMILE nodes, measured with an unmodulated carrier at the input.

V_{out} is the DC output voltage when an unmodulated carrier with power $P_{\text{in}}^{\text{RF}}$ is fed in the input. The parameter V_{slope}, calculated in mV/dB, describes the slope of the I/O characteristic. P_0, measured in dBm, is the so-called log-intercept—the point where the extrapolated linear response would intersect the abscissa. V_{slope} and P_0 are estimated for each sMILE node using curve fitting and the measurements from Fig. 5.

Using (5) it is possible to compute the *envelope of the baseband received signal*, i.e., the signal of interest. This operation requires exponentiation as follows:

$$|V_{\text{in}}(t)| \quad = \quad \sqrt{2} \cdot 10^{\alpha V_{\text{out}}(t)+\beta}, \tag{6}$$

where the parameters α and β are computed according to

$$\alpha = \frac{1}{20 V_{\text{slope}}}, \quad \beta = \frac{P_0 - 13.01}{20}, \tag{7}$$

for every sMILE node separately (cf. [5]). Note that the IF carrier has been removed by the RSSI detector (see [5] for more details).

C. Sampling

So far we discussed the generation of the transmit signal and the extraction of the envelope at the sMILE nodes. The output $V_{\text{out}}(t)$ of the sMILE nodes is fed to a digital oscilloscope which records the received signals. Up to 4 signals can be recorded simultaneously, which limits the testbed to a maximum of 4×4 MIMO. The signals are oversampled at 250 MS/s, a rate which is sufficient for the 25 MHz video output of the RSSI detector. Furthermore, the sampled values are uniformly quantized with 16 bits. The oversampled noisy signals, denoted $\widehat{V}_{\text{out}}[n]$, are then transferred to Matlab, where further processing takes place.

TABLE II
sMILE HARDWARE COMPONENTS (ALL OF SMD TYPE).

	Type	Description
RF Bandpass	DFCB25G59LAHAA	Dielectric Filter $f_c = 5.5975$ GHz, $W_{\text{RF}} = 255$ MHz, image rejection 30 dB
LNA	RF5515	$4.9 - 5.85$ GHz, 11 dB typical gain, NF=1.6 dB
Mixer	MCA1-85L+	Ceramic wide band mixer, $2.8 - 8.5$ GHz
VCO	ROS-5200C-119+	Linear tuning LO $4.975 - 5.363$ GHz, $f_{\text{LO}} = 5.2947$ GHz
IF Amplifier	SGA-3563	DC-5 GHz SiGe HBT MMIC amplifier, 27 dB gain, NF=2.2 dB @ 300 MHz
IF Bandpass	RF3602D	SAW filter, $f_{\text{IF}} = 305.3$ MHz, $W_{\text{IF}} = 12.5$ MHz
RSSI Detector	AD8310	Demodulating logarithmic amplifier, DC–440 MHz, 95 dB dynamic range, $W_{\text{video}} = 25$ MHz

D. Noise Characterization

As mentioned before, the logarithmic amplifiers are not characterized by a single noise figure. Weak signals traverse through several amplification stages and aggregate a lot of thermal noise, while strong signals are amplified by less stages and experience much less noise. After sampling and quantization by the oscilloscope, the noisy quantized samples $\widehat{V}_{\rm out}[n]$ are perturbed by two noise processes: the *thermal noise* as seen at the RSSI output and the *quantization noise*. At $\widehat{V}_{\rm out}[n]$ the noise is dominated by the RSSI operation, while the quantization noise is uniform. However, this is not true for $|\widehat{V}_{\rm in}[n]|$. Due to the exponentiation in (6), the uniform quantization levels of the oscilloscope are now multiplied with the received signal. As a consequence, strong signals suffer from strong quantization noise, while weak signals are compressed and appear less noisy (cf. [5]).

Performing a statistical analysis of the noise in $|\widehat{V}_{\rm in}[n]|$ resulted in two models. Whenever a 'high' level is sampled, i.e., whenever the transmit signal is not equal to zero, the noise is best approximated by a Gaussian or Rician distribution[2]. Note that the theoretical model assumes a Rician pdf. In the case when a 'high' is expected, the signal is first low-pass filtered in order to smoothen the quantization noise (cf. Section III-E). The variance of the Gaussian approximation is a function of the received signal strength, as a consequence of the multiplicative quantization noise. The parameters that best describe the Gaussian noise are

$$\left\{\mu_1, \sigma_1\left(\widehat{|h|}\right)\right\} = \left\{\widehat{|h|},\ 0.004483\widehat{|h|} + 0.0026\right\}, \qquad (8)$$

for all sMILE nodes, where $\widehat{|h|}$ is the estimated norm of the channel during a SISO transmission.

Whenever the transmit signal equals zero, the corresponding sample is in fact only a sample of the noise process. In this case, the noise is best described by a lognormal distribution with parameters:

$$\left\{\mu_0\left(\widehat{|h|}\right), \sigma_0\right\} = \left\{0.478\widehat{|h|} - 5.555,\ 0.4341\right\}, \qquad (9)$$

for all sMILE nodes. Note that the theoretical model in Section II assumes these samples are Rayleigh distributed.

E. Software Receiver

Fig. 6 depicts a block diagram of the software receiver. The received signal $\widehat{\boldsymbol{V}}_{\rm out}[n]$ corresponds to $N_{\rm R}$ noisy recorded signals at the oscilloscope. The various blocks of the software receiver are described below:

Exp: First, the envelopes $|\widehat{V}_{\rm in}[n]|$ are computed from $\widehat{\boldsymbol{V}}_{\rm out}[n]$ using (6). This operation takes place for each received signal separately, using the parameters α and β of the corresponding sMILE nodes.

LP: In order to smoothen the strong quantization noise observed at sampling points that correspond to non-zero transmit signal, a low-pass FIR filter is applied (cf. Sec. III-D). The output, $|\widehat{\boldsymbol{V}}^{\rm f}_{\rm in}[n]|$ is kept alongside the unfiltered version of the signal in the following.

[2]For the given parameters the Rician distribution converges to a Gaussian. We use the Gaussian distribution for the sake of simplicity.

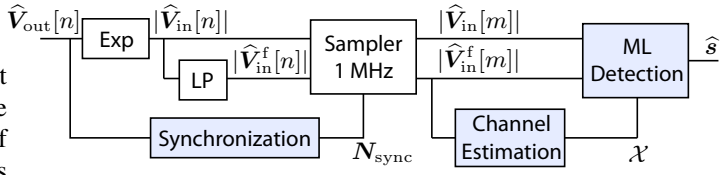

Fig. 6. Block diagram of 'Processing/Detector' cell. Corresponds to MIMO processing of the received signals from all sMILE nodes.

Synchronization: The logarithmic domain received signals $\widehat{\boldsymbol{V}}_{\rm out}[n]$ are correlated with the synchronization sequence in order to determine the optimum sampling points for *each packet*. This operation is executed separately for each oscilloscope channel and the optimal sampling points are stored in $\boldsymbol{N}_{\rm sync}$.

Sampler 1 MHz: Using the determined optimum sampling points, the linear domain oversampled signals $|\widehat{V}_{\rm in}[n]|$ and $|\widehat{V}^{\rm f}_{\rm in}[n]|$ are down-sampled at $f_s = 1$ MHz symbol rate. The new sampling frequency is denoted with the time-index m in Fig. 6.

Channel Estimation: This block uses the filtered version of the down-sampled signal $|\widehat{V}^{\rm f}_{\rm in}[m]|$ and applies the channel estimation algorithms presented in [5] in order to estimate the sufficient CSI $\mathcal{X}$ for every packet.

ML Detection: The ML Detector employs the sufficient CSI and detects the transmitted data bits using both $|\widehat{V}_{\rm in}[m]|$ and $|\widehat{V}^{\rm f}_{\rm in}[m]|$. The ML rule for detecting the ith transmit symbol reads

$$\widehat{\boldsymbol{s}}[i] = \underset{\boldsymbol{s}_m \in \mathcal{S}}{\operatorname{argmax}}\, \Lambda_i(\boldsymbol{s}_m) \qquad (10)$$

and the likelihood function $\Lambda_i(\boldsymbol{s}_m)$ is given by (cf. (1))

$$\Lambda_i(\boldsymbol{s}_m) = \begin{cases} \prod_{j=1}^{N_{\rm R}} {\rm p}_0\left(|\boldsymbol{e}_j^{\rm T}\widehat{\boldsymbol{V}}_{\rm in}[i]|\,\middle|\,\boldsymbol{s}_m\right), & \text{if} \quad \boldsymbol{s}_m = \boldsymbol{0} \\ \prod_{j=1}^{N_{\rm R}} {\rm p}_1\left(|\boldsymbol{e}_j^{\rm T}\widehat{\boldsymbol{V}}^{\rm f}_{\rm in}[i]|\,\middle|\,\boldsymbol{s}_m\right), & \text{if} \quad \boldsymbol{s}_m \neq \boldsymbol{0} \end{cases}, \qquad (11)$$

The pdf ${\rm p}_0(\cdot)$ is lognormal with parameters given in (9) and utilizes the samples $|\widehat{V}_{\rm in}[m]|$, while the pdf ${\rm p}_1(\cdot)$ is Gaussian with parameters given in (8) and uses $|\widehat{V}^{\rm f}_{\rm in}[m]|$.

IV. Operation and Measurements

In this Section we present a series of different measurements and analyze the results. The parameters of the measurements are given in Table III. The last column states the spectral efficiency for the given parameters, computed as

$$\eta = N_{\rm T} \cdot \frac{N_{\rm data}}{N_{\rm SpP}} \cdot \frac{f_s}{W_{\rm pb}} = \frac{N_{\rm T} N_{\rm data}}{2N_{\rm SpP}} \quad [\text{bits/s/Hz}]. \qquad (12)$$

① *Synchronization:* The first two measurements are conducted via cable in order to attain a static channel. We compare the impact on the BER of the 11-Barker code and $(m = 31)$-sequence, in low SNR conditions. The received signal power at the sMILE node is -94 dBm. The long m-sequence leads

TABLE III
TYPICAL SMILE OPERATION PARAMETERS.

	$N_{\mathrm{T}} \times N_{\mathrm{R}}$	Users	Propagation Environment	distance [m]	Synchronization Sequence	N_{SpP}	Chanel Estimation Scheme	N_{pilot}	BER	Spectral Efficiency [bits/s/Hz]
①	1×1	1	cable	-	Barker	250	SEES	20	0.172	0.438.
	1×1	1		-	m-sequ.	250	SEES	20	0.159	0.398
②	2×1	1		-	Barker	250	SEES	10	$6.1 \cdot 10^{-2}$	0.756
	2×2	1		-	Barker	250	SEES	10	0	0.756
③	1×1	1	LOS	20	Barker	250	SEES	10	10^{-3}	0.458
	1×1	1		37^*	Barker	250	SEES	10	0	0.458
	2×2	1		25	Barker	250	SEES	10	$2.5 \cdot 10^{-2}$	0.836
	2×2	1		37^*	Barker	250	SEES	10	$2.5 \cdot 10^{-4}$	0.836
④	3×3	2		10	Barker	150	SEES	6	$3.3 \cdot 10^{-3}$	0.97
	3×3	2		10	Barker	150	GAES	7	$9.5 \cdot 10^{-3}$	0.97
	3×3	2		10	Barker	150	ARES	6	0	0.97
⑤	4×4	2		10	Barker	500	ARES	3	$1.2 \cdot 10^{-2}$	1.8360
	4×4	2		10	Barker	80	ARES	3	$6 \cdot 10^{-5}$	0.9750

as expected to better BER. The erroneous bits are 3852 when the Barker code is used, and 3241 when using the m-sequence.

② *MIMO advantage:* The next two measurements demonstrate the advantage of using multiple receive antennas, by comparing a 2×1 with a 2×2 system. The measurement is arranged such that the received signal on the first antenna is around 21 dB weaker than on the second antenna. As a consequence, it is possible to distinguish between the four different transmitted symbols using only the first received signal, as if we had a 2×1 MISO system. The resulting BER equals $6.1 \cdot 10^{-2}$, and is a result of poor signal to noise ratio and detecting a virtual $(M = 4)-$OOK. If the received signal on the second antenna is also employed during ML detection, as in a regular 2×2 system, the BER is reduced to zero.

③ *Range:* The following four measurements demonstrate the range of the testbed. The measurement environment is a long corridor. At the maximum length of the corridor, $d = 37$ m, the RACooN's transmit power is set to 7.5 dBm. The resulting BER is still very low. For the maximum RACooN transmit power of 23.5 dBm and a target BER of 10^{-2} in the SISO case, the maximum path loss is 112.5 dB. Using a path loss exponent of 3, the theoretical range is then 150 m.

④ *3×3 channel estimation:* The three 3×3 measurements compare the performance of SEES, GAES and ARES with values for certain N_{pilot} values. For the specific choice of N_{pilot}, all three systems have the same spectral efficiency. The BER for all three estimation schemes is low. However, since we deal with wireless transmissions, it is not possible to recreate exactly the same conditions for all three transmissions. Hence, the BER should not be considered as absolute figure of merit.

⑤ *Packet length:* The following two measurements demonstrate the effect of the packet length on the BER. We compare two packet sizes $N_{\mathrm{SpP}} = 500$ and $N_{\mathrm{SpP}} = 80$. All other parameters are identical. When very short packets are used the channel is estimated very often. Hence, the estimated sufficient CSI is usually up-to-date and the BER is very low. However, this compromises the spectral efficiency, which, in this example, is reduced to only one half. When the packet length is long, the sufficient CSI becomes outdated during the duration of the packet, and as a consequence the ML detector yields errors. In fact, the BER is dramatically higher for $N_{\mathrm{SpP}} = 500$, indicating that outdated CSI is a major source of bit errors.

Two important error sources were identified through the experiments: synchronization and channel estimation. At low SNR bad synchronization leads to very high BERs, while outdated CSI in long packets also affects the performance significantly (see measurement ⑤). The testbed was characterized by two–instead of one–noise pdfs and the use of two different signals for detecting 'high' and 'low' levels. This was a result of using an RSSI detector and exponentiating in (6). These effects were implementation-imposed. Despite this, the three channel estimation schemes are still relevant and necessary for estimating the sufficient CSI. Their operation is connected to the limitation of having access only to the envelopes of the received signal, which is a fundamental characteristic of MIMO envelope detection. Finally, the testbed showed the detection of spatially multiplexed OOK streams is possible in a practical system with limited complexity, thus enabling a new design space for low cost/low power MIMO systems.

REFERENCES

[1] D. C. Daly and A. P. Chandrakasan, "An Energy-Efficient OOK Transceiver for Wireless Sensor Networks," *IEEE Journal of Solid State Circuits*, vol. 42, pp. 1003–1011, May 2007.

[2] G. K. Psaltopoulos and A. Wittneben, "Nonlinear MIMO: Affordable MIMO Technology for Wireless Sensor Networks," *IEEE Transactions on Wireless Communications*, vol. 9, pp. 824–832, February 2010.

[3] ——, "Diversity and Spatial Multiplexing of MIMO Amplitude Detection Receivers," in *Proceedings IEEE Personal, Indoor and Mobile Radio Communications Symposium*, September 2009.

[4] ——, "Channel Estimation for Very Low Power MIMO Envelope Detectors," in *Proceedings IEEE International Conference on Communications*, May 2010.

[5] G. K. Psaltopoulos, *Affordable Nonlinear MIMO Systems*. PhD Dissertation, Logos Verlag Berlin, 2011.

[6] S. Berger, *RACooN Lab*. http://www.nari.ee.ethz.ch/wireless/research/projects/racoon/introduction.html.